arXiv:1408.5853v3 [physics.comp-ph] 19 Nov 2015

Algorithm and Simulation of Heat Conduction Process for Design of a Thin Multilayer Technical Device

Alexander Ayriyan[a,*], Ján Buša Jr.[b,c], Eugeny E. Donets[d], Hovik Grigorian[a,e], Ján Pribiš[a,b]

[a] *Laboratory of Information Technologies, JINR, Dubna, Russia*
[b] *Department of Mathematics and Theoretical Informatics, TU of Košice, Košice, Slovakia*
[c] *Institute of Physics, Academia Sinica, Nankang, Taipei, Taiwan*
[d] *Veksler and Baldin Laboratory of High Energy Physics, JINR, Dubna, Russia*
[e] *Department of Theoretical Physics, Yerevan State University, Yerevan, Armenia*

Abstract

A model of a multilayer device with non-trivial geometrical structure and nonlinear dependencies of thermodynamic material properties at cryogenic temperatures is suggested. A considered device, called cryogenic cell, is intended for use in multicharged ion sources for pulse injection of gaseous species into ionization space of ion sources. The main requirement for the cryogenic cell operation is the permanent opening and closing for gaseous species injection in a millisecond range, while cell closing is provided by freezing of the gaseous specie at the outer surface of the cell and the cell opening – by the corresponding pulse heating of the cell surface up to definite temperature. The thermal behaviour of the device in a millisecond time range is simulated. The algorithm for solving the non-stationary heat conduction problem with a time-dependent periodical heating source is suggested. The algorithm is based on finite difference explicit-implicit method. The OpenCL realization of the algorithm is discussed. The optimal particular choice of the parameters to provide the required pulse temperature regime of the designed cryogenic cell for the chosen working gas is presented. Based on these results further optimization can be formulated.

Keywords: Heat evolution, Periodical heating source, Multilayer cylindrical structure, Finite-difference scheme, OpenCL realization,
PACS: 44.10.+i

1. Introduction

In modern science the phenomena of thermal conductivity is a very common technology for studying of complex objects with complex geometric and physical structure. The main goal of this work is to suggest a model of temperature evolution for a multilayer cylindrical object, called cryogenic cell, which has application in sources of multicharged ions [1]. The function of the cryogenic cell is a pulse injection (in the millisecond range) of the working gases into the working space of the ion source.

*Corresponding author
Email address: ayriyan@jinr.ru (Alexander Ayriyan)

In the modern applied thermal engineering the dependences of physical properties of materials on temperature (even in small interval) can ensure elegant way for the diagnosis, monitoring and management of complex systems. Such interesting examples are presented in [2] and [3].

Pulse injection of a gaseous species could be provided by fast mechanical gate valves, however, robust operation in millisecond range in cryogenic environment is out of their possibilities. The use of temperature properties of gases at cryogenic temperatures could be a real alternative to pulse mechanical gate valves in a millisecond range time operation. Indeed, dependency of vapor pressure of all gases on temperature is very strong in a cryogenic temperature range, i.e. between liquid helium temperature 4.2 K and liquid nitrogen temperature 78 K. Typical data for Krypton is given in Table 1 (see [4]).

Table 1: Krypton vapour pressure as a function of temperature

ine Temperature, K	27.9	29.4	30.9	32.7
Krypton vapour pressure, Torr	1.3×10^{-13}	1.3×10^{-12}	1.3×10^{-11}	1.3×10^{-10}
ine				
ine Temperature, K	34.6	36.8	39.3	42.2
Krypton vapour pressure, Torr	1.3×10^{-9}	1.3×10^{-8}	1.3×10^{-7}	1.3×10^{-6}
ine				

It is known in ion sources technology [5], that if a working gas vapour pressure is around 10^{-6} Torr, its typical injection time from the injection cell into the ionization space of ion source is about 1 ms. For example, for Krypton it corresponds to the temperature of 42.2 K. Injection cell in this case should be placed in a vicinity of working space of ion source, about 1 cm aside of ionization region of ion source. Another side, if gas vapour pressure is about 10^{-13} Torr it means that all gas molecules are frozen at the cell surface which has such temperature; for Krypton, for example, this temperature is 27.9 K. This opens possibility to use such temperature dependencies for gas injection in millisecond time range.

One needs to create such cryogenic cell which provides change of its surface temperature from, say 20 K up to, say, 45 K, and back during few milliseconds and with a frequency about 50 Hz.

Some additional requirements for such cryogenic cell construction are inspired by some basic aspects of ion source technology and cryogenic technics:

— there are two natural temperature terminals in cryogenics – liquid helium temperature terminal 4.2 K and liquid nitrogen temperature terminal 78 K, thus it is natural to use such temperature terminals as a thermostats with big capacity;

— cryogenic cell surface should be heated up by pulse electric current, passing through conductive layer in a vicinity of cell surface; in order to prevent disturbances in a working space of ion source it has to be placed in a vicinity of a working ionization space of ion source. The maximal electric current I and through the cell a corresponding voltage should be restricted to $I \times R < 1000$ V, where R is a resistance of the conductive layer.

Design of such cryogenic cell has been elaborated and recently tested in JINR [6, 7]. Which shows, that the cell exhibited expected above mentioned time and temperature parameters. For

the reason of practical use in ion sources one needs to create a sample of cryogenic cell which fits more precisely the time and temperature requirements in millisecond time range at cryogenic temperatures. The present work describes details of numerical strategy, which is used to create suitable numerical tool for optimization of cryogenic cell construction.

So, one needs to simulate thermal process in a cell of a chosen geometry, which is governed by the periodic passage of electric current through one of the layers of the cell. The period of the process is requested to be $t_{\text{prd}} = t_{\text{src}} + t_{\text{clg}}$. Here t_{src} is a period of heating and t_{clg} is a period of cooling down. The period is divided in two parts: when the cell evaporates working gases from its surface ($T > T_{\text{crit}}$) and when the rest of the working gas (which is not penetrated into ion source ionization space) freezes on the surface ($T < T_{\text{crit}}$). The cell itself should work at the cryogenic temperature range from temperature of liquid helium ($T = 4.2\,\text{K}$) up to the temperature of liquid nitrogen. The cell structure has a cylindrical symmetry; therefore, the heat conductivity inside it can be simulated by a model with two spatial cylindrical coordinates, r and z, and time variables (Fig. 1). Similar but more simple model has been discussed in [8] and [9].

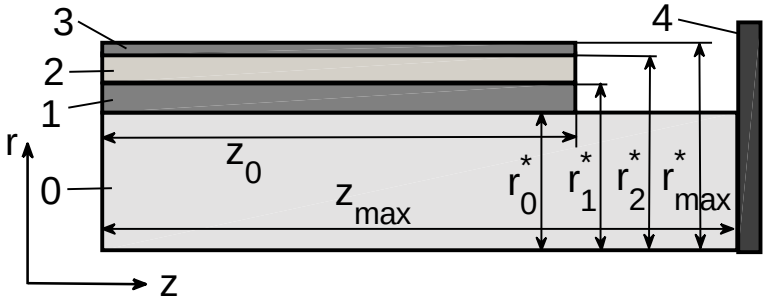

Figure 1: Schematic view of the object half-slice. The bottom line is the axis of a cylinder (axis of the symmetry), $r = 0$. The slice of the object: 0 – cooler, 1 – electrical insulator, 2 – heat source (conductive layer), 3 – external insulator, 4 – liquid helium temperature terminal with $T = 4.2\,\text{K}$.

2. Main Equations and Boundary Conditions

The thermal processes in the object can be described by the following system of parabolic partial differential equations with temperature depended coefficients [10]:

$$\rho_m c_{Vm}(T)\frac{\partial T}{\partial t} = \frac{1}{r}\frac{\partial}{\partial r}\left(r\lambda_m(T)\frac{\partial T}{\partial r}\right) + \frac{\partial}{\partial z}\left(\lambda_m(T)\frac{\partial T}{\partial z}\right) + X_m(T,t), \tag{1}$$

where $r \in [0, r_{\max}(z)]$, $z \in [0, z_{\max}(r)]$ (or $(r,z) \in \Omega$) and $t \geq 0$. The object consists of different materials in construction with different densities and thermal coefficients; thus, the index m is introduced for each material ($m = 0$ – cooler (copper), $m = 1$ – electrical insulator, $m = 2$ – heat source (graphite), $m = 3$ – external insulator). In the frame of this work, physical and engineering needs of the object geometry are not discussed. The source function in Eq. (1) is $X_m(T) \equiv 0$ for the layers $m = 0$,1, and 3 (there is no source) and it has a periodical time dependence:

$$X_2(T,t) = \chi(T)\frac{I^2(t)}{S_2^2}, \tag{2}$$

where S_2 is the cross-sectional area in units of cm^2 and $\chi(T)$ is temperature depended resistivity of the conducted layer $m = 2$. The current can be expressed in the form:

$$I(t) = I_0 \nu(t) p(t), \tag{3}$$

where I_0 is the amplitude of current and $\nu(t)$ represents the time structure:

$$\nu(t) = \begin{cases} 1, & nt_{\text{prd}} \le t < nt_{\text{prd}} + t_{\text{src}}, \\ 0, & nt_{\text{prd}} + t_{\text{src}} \le t < (n+1)t_{\text{prd}}, \end{cases} \tag{4}$$

here $n \in \mathbb{N}_0$ – is index of a period of the electric current. Function $\nu(t)$ has a uniform rectangular waveform (definition of this function one can find in [11]), and $p(t)$ is a model of the transient response function for the turn-on process (it is introduced in analogous with similar function in electrical engineering, see for example [12]). In a simple case, it can be the Heaviside step function. For this work the function $p(t)$ is discussed in Section 3.1. In the formulas, $I(t)$ stands for electric current in the graphite slice along z direction. In a common case, the thermal coefficients are nonlinear functions of the temperature and the spatial coordinates with discontinuities of the first kind (for $m + 1$ materials, there are m points of discontinuities).

The initial condition is given by

$$T(r, z, t = 0) = T_0, \tag{5}$$

where $T_0 \equiv 4.2$ K (liquid helium temperature) and the boundary conditions are taken as

$$\begin{cases} \dfrac{\partial T}{\partial \mathbf{n}} = 0 & \forall\, (r, z) \in \delta\Omega \setminus \{(r, z) : z = z_{\max}\}, \\ T = T_0 & \forall\, (r, z) \in \{(r, z) : z = z_{\max}\}, \end{cases} \tag{6}$$

where $\delta\Omega$ is the boundary of the Ω, and $\mathbf{n}$ is the normal vector of $\delta\Omega$. The temperature at the right side is always equal to T_0 because of contact with liquid helium.

The parameter ρ and the functions c_V, λ, and $X_i = X(T_i)$ have discontinuities of the first kind at the following surfaces with radii: r_0^*, r_1^*, and r_2^* in the interval $[0, r_{\max}]$. Conjugation conditions between materials are considered to be ideal:

$$\begin{cases} T|_{r=r_m^*-0} = T|_{r=r_m^*+0}, \\ -\lambda_m(T) \left.\dfrac{\partial T}{\partial r}\right|_{r=r_m^*-0} = -\lambda_{m+1}(T) \left.\dfrac{\partial T}{\partial r}\right|_{r=r_m^*+0}, \end{cases} \tag{7}$$

where r_m^* are points of the border between the materials m and $m + 1$ (discontinuity points), here $m = 0, 1, 2$.

3. Numerical Algorithm

The initial-boundary value problem Eqs. (1)–(6) has been approximated by the following mixed explicit-implicit finite difference scheme (see [13, 14]):

$$\rho_{i,j}\, c_{V\,i,j} \frac{\widehat{T}_{i,j} - T_{i,j}}{\tau} = \Lambda_i [\, \widehat{T}_{i,j} \,] + \Lambda_j [\, T_{i,j} \,] + X_{i,j}, \tag{8}$$

where $\widehat{T}_{i,j}$ is the temperature on the next time step, $T_{i,j}$ is the temperature on the current time step, τ is the time-step.

Numerical solution of Eq. (8) can be obtained using a special non-uniform grid:

$$\begin{aligned}\overline{\omega} \;= \{(t,x,z)\,|\quad & 0 \le t < \infty, \quad t_i = k \cdot h_t, \quad k \in \mathbb{N}_0; \\ & 0 \le r \le r_{\max}, \quad r_{i+1} = r_i + h_{i+1}, \quad i = 0,\ldots,N_j - 1; \\ & 0 \le z \le z_{\max}, \quad z_{j+1} = z_j + \eta_{j+1}, \quad j = 0,\ldots,M_i - 1\}.\end{aligned} \tag{9}$$

The spatial finite difference operator is:

$$\Lambda_i\,[\,\widehat{T}_{i,j}\,] = \frac{1}{r_i}\frac{1}{\hbar_i}\left[r_{i+\frac{1}{2}}\lambda_{i+\frac{1}{2},j}\frac{\widehat{T}_{i+1,j} - \widehat{T}_{i,j}}{h_{i+1}} - r_{i-\frac{1}{2}}\lambda_{i-\frac{1}{2},j}\frac{\widehat{T}_{i,j} - \widehat{T}_{i-1,j}}{h_i}\right], \tag{10}$$

$$\Lambda_j\,[\,T_{i,j}\,] = \frac{1}{\eta_j}\left[\lambda_{i,j+\frac{1}{2}}\frac{T_{i,j+1} - T_{i,j}}{\eta_{j+1}} - \lambda_{i,j-\frac{1}{2}}\frac{T_{i,j} - T_{i,j-1}}{\eta_j}\right], \tag{11}$$

where $i = 1,\ldots,N_j - 1$, $j = 1,\ldots,M_i - 1$, $h_i = r_i - r_{i-1}$, $\eta_j = z_j - z_{j-1}$, $\hbar_i = (h_{i+1} + h_i)/2$, $\eta_j = \left(\eta_{j+1} + \eta_j\right)/2$, $T_{i,j} = T(r_i, z_j, t_k)$, $\widehat{T}_{i,j} = T(r_i, z_j, t_{k+1})$, $\lambda_{i,j} = \lambda_m(T_{i,j})$, $c_{V\,i,j} = c_{V\,m}(T_{i,j})$, $X_{i,j} = X_m(T_{i,j})$, $r_{i\pm\frac{1}{2}} = (r_i + r_{i\pm1})/2$, $\lambda_{i\pm\frac{1}{2},j} = \lambda_m(T_{i,j} + T_{i\pm1,j})/2$, $\lambda_{i,j\pm\frac{1}{2}} = \lambda_m(T_{i,j} + T_{i,j\pm1})/2$.

The indices i and j are global for the whole computational domain. The index m, which marks the material, is chosen correspondingly to the domain region, from which the pair $(i,\ j)$ is taken.

The coefficients for the forward sweep of the Thomas algorithm described in [15, 16] are defined as:

$$\begin{cases} \alpha_i = \dfrac{-C_i}{B_i + A_i\alpha_{i-1}}, \\ \beta_i = \dfrac{F_i - A_i\beta_{i-1}}{B_i + A_i\alpha_{i-1}}. \end{cases} \tag{12}$$

The coefficients A_i, B_i, C_i, and F_i are formulated from the difference equation (8):

$$\begin{cases} A_i = \dfrac{-r_{i-\frac{1}{2}}\lambda_{i-\frac{1}{2},j}}{r_i\,\hbar_i\,h_i}, \\ B_i = \dfrac{1}{r_i\hbar_i}\left[\dfrac{r_{i-\frac{1}{2}}\lambda_{i-\frac{1}{2},j}}{h_i} + \dfrac{r_{i+\frac{1}{2}}\lambda_{i+\frac{1}{2},j}}{h_{i+1}}\right] + \dfrac{\rho_{i,j}\,c_{V\,i,j}}{\tau}, \\ C_i = \dfrac{-r_{i+\frac{1}{2}}\lambda_{i+\frac{1}{2},j}}{r_i\,\hbar_i\,h_{i+1}}, \\ F_i = \dfrac{\rho\,c_{V\,i,j}}{\tau}T_{i,j} + \Lambda_j\,[\,T_{i,j}\,] + X_{i,j}. \end{cases} \tag{13}$$

Finally, the following formula has been used to calculate unknown values of $\widehat{T}_{i,j}$:

$$\widehat{T}_{i,j} = \alpha_i\widehat{T}_{i+1,j} + \beta_i. \tag{14}$$

For the forward sweep Eqs. (12)–(13) and back sweep Eq. (14), one needs to initialize values α_0, β_0, and $\widehat{T}_{N_j,j}$ respectively. These values have to be initialized to satisfy the boundary conditions.

It is known (see [10, 13]) that in the case of a non-uniform grid or discontinuities of the first kind of the thermal coefficients, Scheme (8) has the first order difference approximation via spatial coordinates[1]. Therefore, for approximations of the boundary and conjugation conditions, it is enough to use the difference approximation of the first order.

The boundary conditions have been approximated by the following set of formulas:

$$\begin{cases} \widehat{T}_{0,j} = \widehat{T}_{1,j}, \\ \widehat{T}_{N_j,j} = \widehat{T}_{N_j-1,j}, \end{cases} \tag{15}$$

for $r = 0$ and $r = r_{\max}$, respectively. Difference approximations of the other boundary conditions can be constructed in a similar way.

The initial values of α and β satisfying the boundary conditions (15) are defined by:

$$\alpha_0 = 1, \;\; \beta_0 = 0. \tag{16}$$

To initialize the recursive formula (14), taking into account the boundary conditions from Eq. (15), the $T_{Nr,j}$ is calculated as:

$$\widehat{T}_{N_j,j} = \frac{\beta_{N_j-1}}{1 - \alpha_{N_j-1}}. \tag{17}$$

The relations on the border between layers are given in the form

$$\begin{cases} \widehat{T}_{i^*-0,j} = \widehat{T}_{i^*+0,j}, \\ -\lambda_m(T_{i^*-0,j})\dfrac{T_{i^*,j} - T_{i^*-1,j}}{h_{i^*}} = -\lambda_{m+1}(T_{i^*+0,j})\dfrac{T_{i^*+1,j} - T_{i^*+0,j}}{h_{i^*+1}}. \end{cases} \tag{18}$$

Here we use the following notation: $\widehat{T}_{i^*,j} = \widehat{T}_{i^*-0,j} = \widehat{T}_{i^*+0,j}$ and $\lambda^*_m = \lambda_m(T_{i^*,j})$. Instead of the recursive formula Eq. (14), after a simple transformation, a similar function can be expressed at the discontinuity point as:

$$\widehat{T}_{i^*,j} = \alpha_{i^*}\widehat{T}_{i^*+1,j} + \beta_{i^*}. \tag{19}$$

From Eq. (18), the coefficients for the forward sweep of the Thomas algorithm α_{i^*} and β_{i^*} can be represented as follows:

$$\begin{cases} \alpha_{i^*} = \dfrac{\lambda^*_{m+1}h_{i^*}}{\lambda^*_{m+1}h_{i^*} + \lambda^*_m h_{i^*+1}(1 - \alpha_{i^*-1})}, \\ \beta_{i^*} = \dfrac{\lambda^*_m h_{i^*+1}\beta_{i^*-1}}{\lambda^*_{m+1}h_{i^*} + \lambda^*_m h_{i^*+1}(1 - \alpha_{i^*-1})}. \end{cases} \tag{20}$$

The difference scheme (8)–(20) has unconditional stability related to spatial step h_i and conditional stability related to η_j (see [14]):

$$\tau \le \frac{\min\left|\eta_j^2\right|}{2} \min\left|\frac{\rho(T,r,z)c_V(T,r,z)}{\lambda(T,r,z)}\right|. \tag{21}$$

[1] Actually, the order of difference approximation depends on the choice of a norm, as it is shown in given references.

Generally, the conditional stability could be a strong limitation for the practical usage of a difference scheme. However, our scheme is practical in the cases, where spatial step is sufficiently large in one direction; moreover, where the step in other direction is too small; and that is the case of our model.

Of course, one could discuss the Alternating Direction Implicit (ADI) method (descibed in [10, 16, 17]) which is absolutely stable with relation to the choice of spatial step. The motivation for our choice of method derives from the relative simplicity of the technical realization when compared to ADI and the natural affinity for parallel computing (parallelization in direction when it has conditional stability).

3.1. Model of Transient Process for Source Term

Generally, for implicit difference schema with coefficients depending on the sought-after function (temperature), one needs to make iterations for evaluation of temperature at each time step (for example, using the Newton method) [10].

Without using iterations, implementation of the Schema (8)–(20) at the moment of noncontinuous switch on of the source (like a theta function) can lead to a jump of the temperature depending on the amplitude of the source (see Fig. 3b). Of course, the choice of sufficiently small time-step will avoid that problem without using iterations. However, we introduce another more physically motivated method to solve this problem, namely the transient process, to avoid sharp behavior of temperature at the switching on of the source.

Formally, it can be done with a choice of the function (Fig. 2)

$$p^2(t) = \begin{cases} 1 - \exp\left(\dfrac{t - nt_{\text{prd}}}{7\tau^*}\right), & nt_{\text{prd}} \le t < nt_{\text{prd}} + \tau, \\ 1, & \text{otherwise}, \end{cases} \tag{22}$$

instead of $p^2(t) \equiv 1$. Here $\tau^* = \tau/100$ and the number 7 is introduced to have saturation occurring approximately in the middle of the time interval τ (7 is a magic number in relation to 100). Note that we choose this function to be suitable for numerical calculation.

The suggested of transient process is simulated in the following way. When the source is switched on (see Eq. (4)), it starts at each moment $t = nt_{\text{prd}}$. We performe the calculations with time-step τ^* up to $t = nt_{\text{prd}} + \tau$. Further, calculations continue with time-step τ and $p^2(t) \equiv 1$ up to $t = (n+1)t_{\text{prd}}$. Then the transient process repeats.

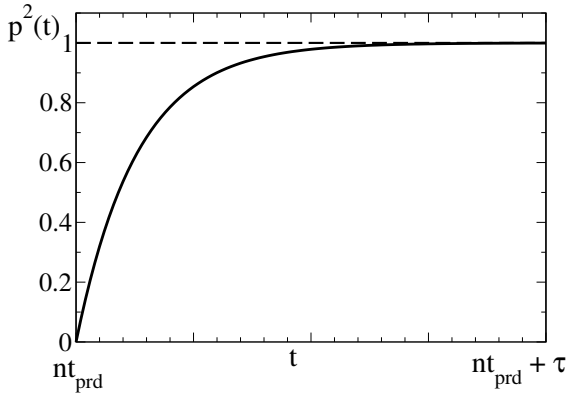

Figure 2: Transient model function $p^2(t)$.

In Fig. 3, comparison between two calculations made with (left figure) and without (right figure) the transient model is shown. Even the behavior of the solutions is completely different. In the incorrect solution (without transient model, Fig. 3b), the

temperature has a big jump and then the system starts cooling down instead of monotonic heating, which is the correct solution (with the transient model, Fig. 3a). The implementation of the transient model method shows that this model is very economical.

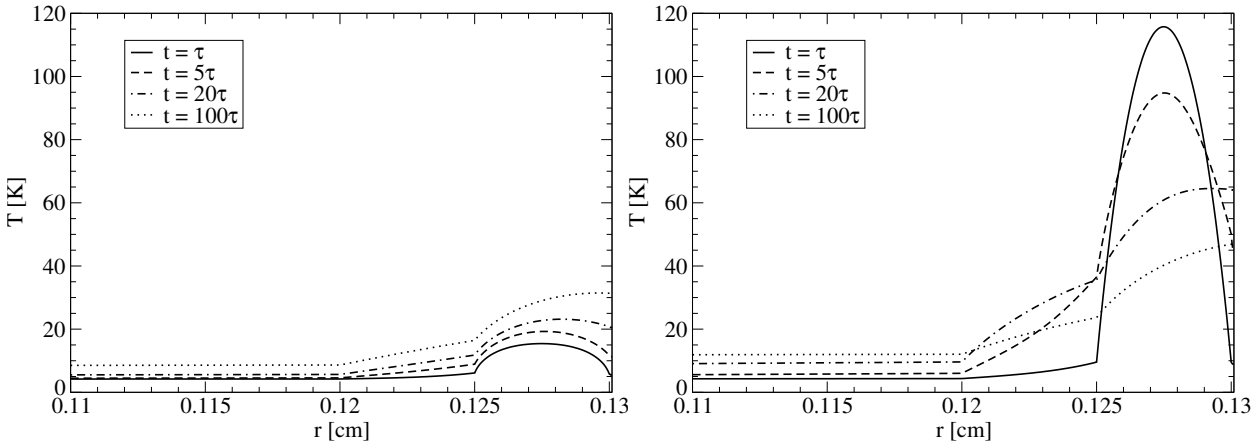

(a) with the transient model

(b) without the transient model

Figure 3: Comparison calculations with transient model and without it for τ, 5τ, 20τ, and 100τ, where τ is the time step of the difference scheame.

4. OpenCL Realization of the Algorithm

The OpenCL realization of the numerical algorithm, described in the previous section, is based on the following idea. In each time step, the cycle for j-index from 1 to $M-1$ is parallelized. Each called thread simultaneously calculates the sought-after function by the Thomas algorithm, see Fig. 4. In the figure, we show the discretization of the function domain. Particularly, we group a set of points corresponding to one j^{th} thread. We also show the points involved in the calculation of the given (i, j) point (circled point and crossed points on the Fig. 4).

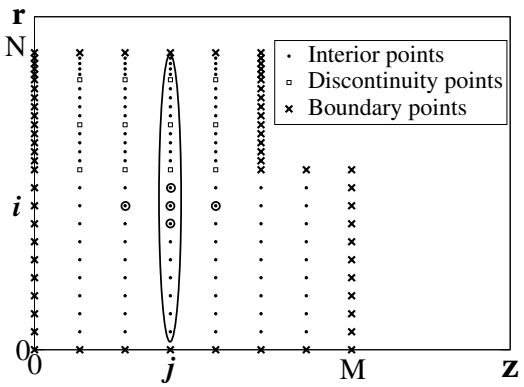

Figure 4: Schematic representation of discretization of the function domain.

5. Results and Discussion

In this work we discuss the results of the numerical simulations only for one particular choice of the configuration of the object (Fig. 1). Its geometrical characteristics have been taken as follows: $r_0 = 0.12\,\text{cm}$, $r_1 = 0.125\,\text{cm}$, $r_2 = 0.13\,\text{cm}$, $r_{\max} = 0.1301\,\text{cm}$, $z_0 = 4\,\text{cm}$, $z_{\max} = 5\,\text{cm}$.

The temperature dependencies of thermal coefficients, c_{Vm} specific heat capacity and λ_m thermal conductivity, for each materials are given as it is shown in Fig. 5. For the chosen materials the corresponding data points have been taken from [18]. These dependencies have been fitted by the least-squares method using polynomial functions:

$$c_{Vm}(T) = \sum_{k=0}^{3} a_k^m\, T^k \tag{23}$$

$$\lambda_m(T) = \sum_{k=0}^{4} b_k^m\, T^k \tag{24}$$

The fit coefficients a_k^m and b_k^m are presented in the Table 2 and Table 3 correspondingly for each material m. The fit functions of thermal coefficients can be used for the temperature range from 4.2 K up to 60 K.

Table 2: The fit coefficients of heat capacity $c_{Vm}(T)$ Eq. (23).

ine m	a_3	a_2	a_1	a_0
0	0.0	4.541×10^{-4}	-3.821×10^{-3}	10^{-2}
1	-6.514×10^{-7}	1.057×10^{-4}	2.366×10^{-2}	-6.619×10^{-3}
2	-8.199×10^{-7}	2.328×10^{-5}	-1.245×10^{-4}	2.169×10^{-4}
3	0.0	0.0	2.35×10^{-2}	2.0×10^{-2}
ine				

Table 3: The fit coefficients of thermal conductivity $\lambda_m(T)$ Eq. (24).

ine m	b_0	b_1	b_2	b_3	b_4
0	7.029×10^{-7}	-9.317×10^{-5}	2.306×10^{-3}	1.166×10^{-1}	-1.139×10^{-1}
1	0.0	-2.523×10^{-7}	2.038×10^{-5}	-1.248×10^{-4}	6.77×10^{-3}
2	0.0	3.03×10^{-9}	-6.369×10^{-7}	1.05×10^{-4}	-2.729×10^{-4}
3	0.0	0.0	0.0	0.0	10^{-3}
ine					

The least-squares fitting of the conducted layer resistivity gives:

$$\chi(T) = \frac{1.8}{\sqrt{T}}\ \text{Ohm} \cdot \text{cm}. \tag{25}$$

For the external insulator (fourth material: $m = 4$), we took the thermal conductivity to be constant $\lambda_3 = 10^{-3}$ W/(cm · K). The densities of the chosen materials are $\rho_0 = 8.92$, $\rho_1 = \rho_2 = 2$ and $\rho_3 = 2.5$ in units g/cm^3.

It is easy to see that thermal coefficients vary up to a few orders of magnitude as temperature varies in cryogenic diapason. It makes the choice of the time-step more sensitive to the values of temperature (sought-after function) (see condition (21)), for this concrete configuration, the suitable time-step is $\tau = 10^{-5}$ s. The period of source switching is $t_{\text{prd}} = 25$ ms, where the heating time is $t_{\text{src}} = 1$ ms – Eq. (4), and electric current amplitude is $I_0 = 363$ mA – Eq. (3). The critical value of temperature is taken as $T_{\text{crit}} = 42.2$ K (temperature of evaporation of working gases). The initial temperature has been taken to be equal $T_0 = 4.2$ K.

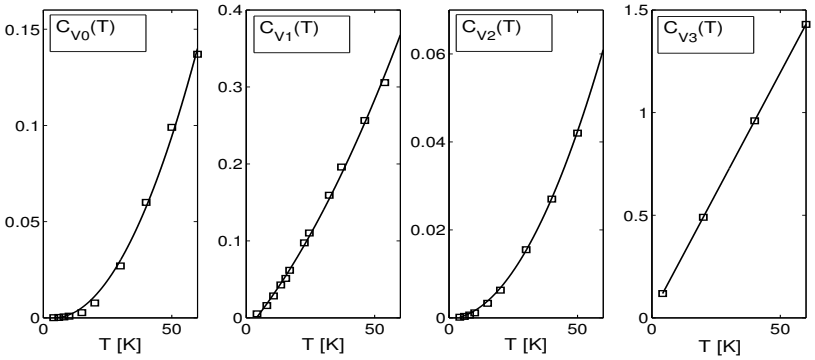

(a) The heat capacities for different materials, $c_V(T)$ [J/(g · K)]. Squares are data points and solid lines are fit functions Eq. (23).

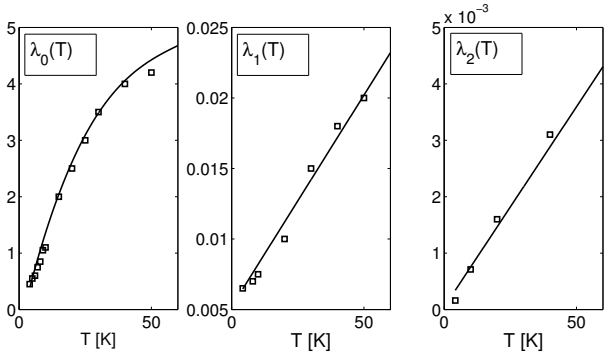

(b) The thermal conductivities for different materials, $\lambda(T)$ [W/(cm · K)]. Squares are data points and solid lines are fit functions Eq. (24).

Figure 5: Temperature dependencies of thermal coefficients.

Note that due to the structural features of the object, especially due to the existence of tiny layers covering the core cylinder, the choice of spatial step in the radial direction has to be smaller in comparison to the size of the layers (at least in order of magnitude) to guarantee the stability of the solution. Therefore, our choice of the difference scheme (see Section 3), which is suitable for the technical realization, is justified.

5.1. Results of Numerical Simulations

In Fig. 6 we show the temperature profiles at the very beginning. The temperature inside the object at $t = 1$ ms is shown in the left (Fig. 6a). At the same moment, the source is switching off

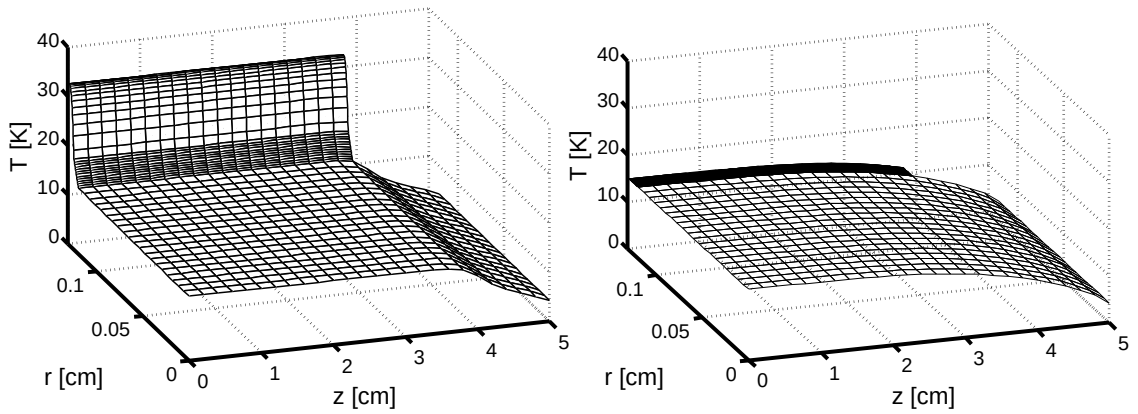

(a) At $t = 1$ ms after switching on the heat source at the very beginning.

(b) At $t = 25$ ms before switching on the heat source of the next period.

Figure 6: Temperature profile $T(r, z)$ at different times.

in the first period of source function. Because the radius of the cylinder is much smaller than its length, the heat first flows to the central axis and then to the right border, where the cryostat (the liquid helium temperature terminal) is located at $z_{\max} = 5$ cm.

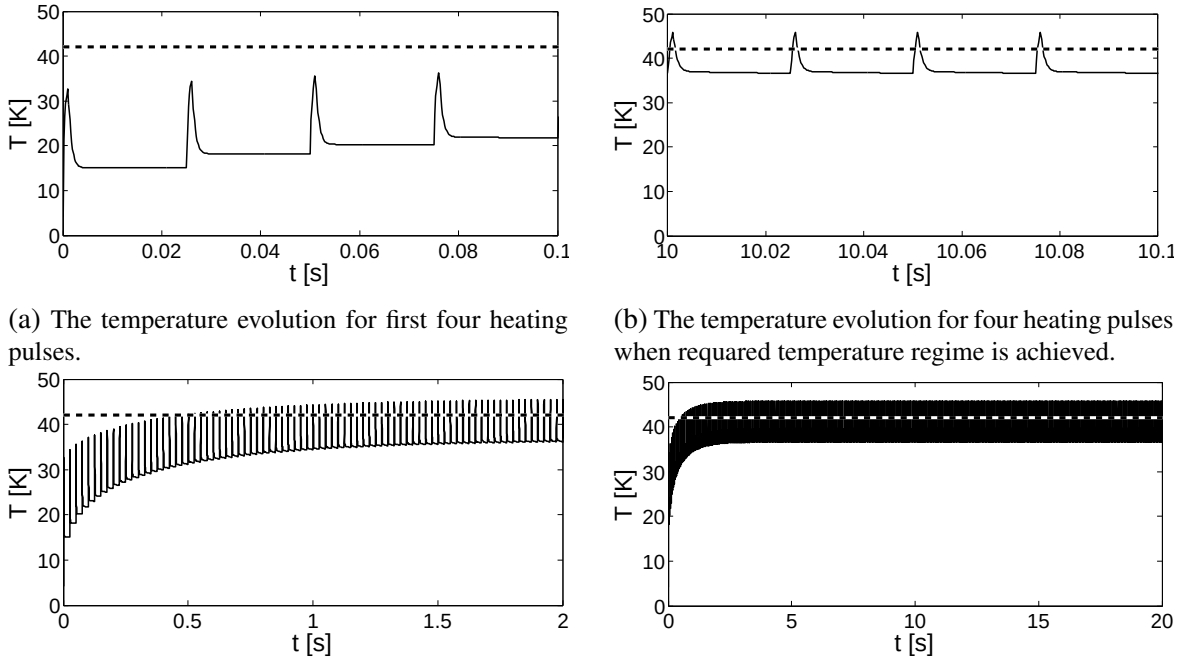

(a) The temperature evolution for first four heating pulses.

(b) The temperature evolution for four heating pulses when requared temperature regime is achieved.

(c) The temperature evolution at the beginning up to $t = 2$ s.

(d) The temperature evolution for all period of simulation.

Figure 7: The evolution of the surface temperature at $(r = r_{\max}, z = 0)$ (solid line). The critical temperature for evaporator and condensation of working gas (dashed line).

In the Fig. 6b we show the temperature distribution at $t = 25$ ms (after first period). One period

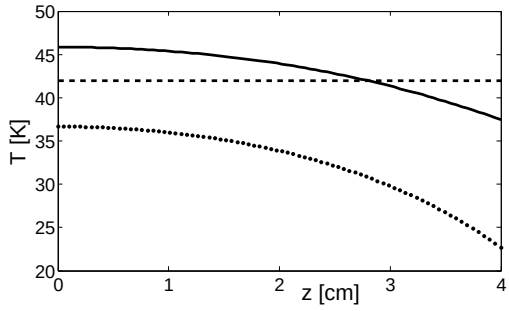

Figure 8: The surface temperature profiles ($r = r_{\max}$) at the stable regime just before at moments of source switching on (dot line) and switching off (solid line). Dashed line is the critical temperature.

of the source switching T_{prd} is the sufficient time to equilibrate the temperature in radial direction (see Fig. 6b). On the other hand, the period of time is not sufficient to relax the temperature to the value right before switching on the source (see Figs. (7a)–(7c)). Such behavior repeats for approximately 10 sec (setting time) until a stable periodic regime is achieved (see Fig. 7d). The setting time varies depending on the design of the object and switching time of the source.

For applications it is very important that the maximum value of the temperature $T_{\max}$ achieves higher value than the critical value of evaporation of working gases ($T_{\text{crit}} \simeq 42.2\,\text{K}$) and is distributed along almost the whole working surface ($r = r_{\max}$, $z \in [0, z_0]$) (Fig. 8). The maximum value of the minimal temperature in the stable regime is less than the critical one (Fig. 8), as it is required.

Moreover, the width of the temperature peaks is approximately 1–1.5 ms and is much smaller in comparison with the whole period (Fig. 7b), which allows for working gases to condensate on the surface before the next evaporation.

In the Fig. 8 it is easy to see, that in our particular case, approximately 75% of the working surface is actually useful. This percentage can be controlled, for example, with a proper choice of the amplitude of electric current I_0. In principle, this equation can be formulated mathematically as source control problem, which can help to raise the efficiency.

5.2. Results of the OpenCL Implementation

The time calculations for different $N \times M$ are given in the Table 4 (here and in the table: $N = \max_{\forall j} N_j$ and $M = \max_{\forall i} M_i$). To demonstrate the results of OpenCL algorithm, the calculations have been carried out for temperature evolution from $t = 0\,\text{s}$ up to $t = 0.025\,\text{s}$ with time step $\tau = 2.5 \times 10^{-7}\,\text{s}$. In the table we use the following notations: CPU – Intel Xeon E5-2695 and GPU – nVidia Tesla K40s. During the compilation of programs -O3 optimization flag has been used. The calculations have been done on the cluster HybriLIT [19]. In the Table 4 we compare the calculation times for CPU and GPU and the speedup using 6 different grids with the same $N = 631$ and various M. It is shown that for the very rare grid the calculation time for both CPU and GPU are the same, however, there is an interval of increasing number of points of discretization in axial direction (M), where the calculation time using GPU remains the same. Therefore, the choice of our algorithm allows us to increase the density of our computational grid in the axial direction, practically without loss of calculation time.

Table 4: Calculation time of OpenCL implementation for different grid size.

ine $N \times M$	631×201	631×401	631×601	631×801	631×1001	631×1201
ine T_{CPU}, min.	13.0	28.8	40.5	44.9	54.9	64.0
T_{GPU}, min.	12.9	14.1	13.0	13.0	13.0	12.9
$T_{\mathrm{CPU}}/T_{\mathrm{GPU}}$	1.009	2.043	3.107	3.454	4.226	4.951
ine						

6. Summary and Conclusions

We have suggested a model of temperature evolution for a multilayer cylindrical object, the cryogenic cell for pulse injection (in millisecond range) of the gaseous working species into the working space of the ion source.

The algorithm for simulation of heat conduction process with a periodical source in cylindrical multilayer object and its OpenCL realization have been developed. It is based on explicit–implicit method. The choice of the difference scheme is suitable for the technical realization (because of the structural features of the cryogenic cell). For the stability of simulations, the transient process model for source switching is introduced.

It was shown that the temperature regime in the cryogenic cell can be conditionally divided in two parts. The first part is the setting mode (around 10 s), in which the required temperature regime at the surface of the cell has not been reached yet. The second part is the working mode, in which the required temperature regime at the surface has already been reached.

The mean value of the temperature over the surface changes around the critical one periodically in the interval of $32\,\mathrm{K} \lesssim T \lesssim 43.5\,\mathrm{K}$ ($T_{\mathrm{crit}} = 42.2\,\mathrm{K}$). The key characteristics of the cell has been achieved by a particular choice of the model parameters, i.e. the conducting (heating) layer material, its thicknesses and source characteristics.

We can conclude that:

— The introduced multilayer object (the cryogenic cell) could be a real alternative to mechanical gate valves for the millisecond pulse injection.

— The suggested algorithm allows to achieve stable solution for all process even in case of the fast oscillation of source.

— The time of setup mode is much longer than a period of the injection time. This feature has to be taken into account in future design and operation of the cryogenic cell.

— The simulation shows that the optimal choice of the cell layer materials, thicknesses and source characteristics provides the required pulse temperature regime on 75% of the working surface of the cryogenic cell.

As an outlook one can mention that further optimization could be done with a variation of the materials and geometry of the cell.

Acknowledgements

Authors thank Dr. Edik Ayryan (JINR), Dr. Ján Buša, Dr. Imrich Pokorný (TU of Košice, Slovakia), Mark A. Kaltenborn, and Prof. David Blaschke (University of Wrocław, Poland) for useful advice and technical help. The research was supported by JINR grant No. 14-602-01 and RFBR grants No. 14-01-00628 and No. 14-01-31227.

References

[1] D.E. Donets, E.D. Donets, E.E. Donets, V.V. Salnikov, V.D. Shutov, Production of Highly Charged Ion Beams Kr32+, Xe44+, Au54+ with Electron String Ion Source (ESIS) Krion-2 and Corresponding Basic and Applied Studies, Journal of Instrumentation 5 (2010) C09001, doi: 10.1088/1748-0221/5/09/C09001.

[2] Su-Heon Jeong, Sung-Ki Nam, Wataru Nakayama, Sun-Kyu Lee, New design of a liquid bridge heat switch to ensure repetitive operation during changes in thermal conditions, Applied Thermal Engineering 59 (2013) 283–289, doi: 10.1016/j.applthermaleng.2013.05.027.

[3] J. Franco, D. Martins, I. Catarino, G. Bonfait, Narrow gas gap in cryogenic heat switch, Applied Thermal Engineering 70 (2014) 115–121, doi: 10.1016/j.applthermaleng.2014.04.062.

[4] R.E. Honig and H.O. Hook, Vapor Pressure Data for Some Common Gases, RCA Review 21(3) (1960) 360–368.

[5] Physics and Technology of Ion Sources, Ed. by I.G. Brown, J. Wiley & Sons, New York, US (1989).

[6] D.E. Donets, E.E. Donets, T. Honma, K. Noda, A.Yu. Ramzdorf, V.V. Salnikov, V.B. Shutov, E.D. Donets, Physics Research and Technology Developments of Electron String Ion Sources, Rev. Sci. Instrum. 83 (2) (2012) 02A512, doi: 10.1063/1.3678660.

[7] A.Yu. Boytsov, D.E. Donets, E.D. Donets, E.E. Donets, K. Katagiri, K. Noda, D.O. Ponkin, A.Yu. Ramzdorf, V.V. Salnikov, V.B. Shutov, Electron string ion sources for carbon ion cancer therapy accelerators, Rev. Sci. Instrum. 86 (2015) 083308, doi: 10.1063/1.4927821.

[8] A. Ayriyan, J. Pribiš, Mathematical Simulation of Heat Conductivity in Composite Object with Cylindrical Symmetry, Matem. model. 24 (12) (2012) 113–118, `mi.mathnet.ru/eng/mm3232` (in Russian).

[9] A. Ayriyan, E. Ayryan, E. E. Donets, J. Pribiš, Numerical Simulation of Heat Conductivity in Composite Object with Cylindrical Symmetry, Lect. Notes Comput. Sci. 7125 (2012) 264–269, doi: 10.1007/978-3-642-28212-6_31.

[10] A.A. Samarskii, P.N. Vabishchevich, Computational Heat Transfer, Volume 1, John Wiley & Sons Ltd., Chichester, UK (1995).

[11] P. Symons, Digital Waveform Generation, Cambridge University Press, New York, US (2013).

[12] Z. Gajic, Linear Dynamic Systems and Signals, Prentice Hall, Upper Saddle River, US (2002).

[13] A.A. Samarsky, The Theory of Difference Schemes, Marcel Dekker Inc., New York, US (2001).

[14] N.N. Yanenko, Fractional step methods for solution of multidimensional problems of mathematical physics, Nauka, Moscow, USSR (1967) (in Russian).

[15] L.H. Thomas, Elliptic Problems in Linear Differential Equations over a Network, Watson Sci. Comput. Lab Report, Columbia University, New York, US (1949).

[16] W.H. Press, S.A. Teukolsky, W.T. Vetterling, B.P. Flannery, Numerical Recipes, third ed., Cambridge University Press, New York, US (2007).

[17] D.W. Peaceman, H.H. Rachford Jr., The Numerical Solution of Parabolic and Elliptic Differential Equations, J. Soc. Ind. Appl. Math. 3 (1) (1955) 28–41, doi: 10.1137/0103003.

[18] National Institute of Standards and Technology, `www.nist.gov` (23/09/2010).

[19] Heterogeneous Computing Cluster HybriLIT, `hybrilit.jinr.ru/en` (11/01/2015).